Adsorption of Graphene to Nickel (111) Using the Exchange-Hole Dipole Moment Model

Matthew S. Christian[a], A. Otero-de-la-Roza[b], Erin R. Johnson[a,*]

[a]*Department of Chemistry, Dalhousie University, 6274 Coburg Road, Halifax, Nova Scotia, Canada B3H 4R2*
[b]*Department of Chemistry, University of British Columbia, Okanagan, 3247 University Way, Kelowna, British Columbia, Canada V1V 1V7.*

Abstract

Graphene is a promising material for a number of technological applications due to its unique electronic properties. It can be mass produced by depositing carbon atoms on metal scaffolds, such as nickel. This work presents a detailed study of graphene adsorption on the nickel (111) surface using the exchange-hole dipole moment (XDM) dispersion correction. XDM is shown to accurately model graphene-nickel interactions, providing adsorption energies in excellent agreement with available experimental data and with RPA calculations. All six graphene-nickel orientations studied present a physisorption energy minimum, but only three exhibit chemisorption. The physisorption and chemisorption minima are close in energy, and are separated by a barrier of $\sim$ 1 kJ/mol per carbon. The relative strength of the chemisorption and physisorption interactions is found to depend heavily on the nickel lattice constant. Thermal expansion stabilizes chemisorption relative to physisorption. The pairwise dispersion coefficients depend strongly on the graphene-nickel distance, and their variation is determined by the exchange-hole dipole moments. If this dependence of the dispersion coefficients with the environment is properly captured, a pairwise dispersion correction (like XDM) is suitable to model surface adsorption.

1. Introduction

Graphene and its potential applications have received much attention over the past decade. Interest in this material grew as a result of the seminal investigation by Novoselov et al., in which

*Corresponding author, E-mail: erin.johnson@dal.ca (Erin R. Johnson)

the authors presented an experimental procedure, the "scotch-tape" method, to isolate high-quality stable graphene layers from graphite[1]. In the past few years, numerous papers have detailed graphene's unique electronic structure and properties[1–14]. Though the scotch-tape method is well suited to creating laboratory samples of graphene, the process is not applicable in the industrial scale. A promising scalable method for commercial graphene manufacturing involves depositing carbon atoms on metallic scaffolds,[15–18] via processes such as chemical vapor deposition (CVD).

In the CVD method, small molecules, such as methane and ethanol, are vaporized at high temperature ($\sim$ 1000 K). The resulting carbon soot is deposited on a metal surface, producing a single monolayer of adsorbed graphene. Once the monolayer is synthesized, a polymer resin is applied to the graphene surface and the metal is typically removed with an acid bath. The graphene layer can then be transferred to the desired substrate and the polymer resin dissolved.[16, 19–21] Nickel is an excellent substrate for graphene synthesis because it is both inexpensive and its (111) surface has cell dimensions commensurate with graphene.[22–26] It has been shown that multilayer graphene can be manufactured similarly, although the exact mechanism as to how multilayers form is still under debate[6, 14, 16, 20].

Multiple studies of the graphene-nickel system using density-functional theory (DFT) have been published[26–33]. These articles show that the generalized gradient approximation (GGA) functionals alone grossly fail to predict experimental adsorption energies and geometries of the graphene-nickel system because GGAs do not adequately describe London dispersion interactions. Even when dispersion interactions are taken into account (e.g. by using one of the multiple available dispersion corrections[34–39]), reproducing the experimental graphene-nickel adsorption energies and interlayer distances is a challenge[27–30]. The difficulties arise from the competing factors that determine the nature of the metal-graphene interaction in this system. Experimentally, graphene is known to chemisorb on the nickel (111) surface[22, 40]; its adsorption energy and distance depend critically on a fine balance between Pauli repulsion, dispersion, and the strength of the incipient chemical bond between graphene and the metal surface[41].

The random-phase approximation (RPA) method[26, 42] is a significant improvement over both the local density approximation (LDA) and GGA functionals regarding the calculation of

intermolecular interactions. Unlike dispersion-corrected GGAs, RPA incorporates dispersion interactions in a non-empirical seamless fashion, albeit at a much higher computational cost. Mittendorfer *et al.*[26] and Olsen *et al.*[42] used RPA calculations to show that graphene not only chemisorbs on nickel, but also physisorbs at larger interlayer distances, giving the adsorption potential energy surface (PES) a characteristic double-minimum profile, with the chemisorption and physisorption minima being very close in energy. Since RPA is too expensive for large surface models, GGA-based functionals have been proposed in the past that include dispersion either via an explicit non-local correlation contribution[43–45] or by adding a dispersion energy correction[37–39, 46–49]. Janthon *et al.*[27] recently examined the ability of several of these density functionals to predict the graphene-nickel adsorption energy. Good adsorption energies and interlayer distances were obtained with optB86b-vdW[44, 50] and DFT-D[48]. The latter is somewhat surprising given that both vdw-TS and DFT-D overestimate the strength of molecular physisorption on noble metal surfaces.[51–53] More recent developments of the same functionals (DFT-D3 and MBD) offer better performance[54].

In this paper, we investigate the adsorption of graphene on nickel (111) using GGA functionals combined with the exchange-hole dipole moment (XDM) dispersion correction[39, 46, 55–57]. XDM has been previously shown to accurately model a wide variety of systems where dispersion interactions play an important role: small noble gas clusters[58, 59], molecular dimers[60–62], supramolecular systems[63], and molecular crystal absolute[64] and relative lattice energies[65, 66]. More relevant to this paper, we have demonstrated previously that XDM successfully predicts physisorption of molecules to surfaces[67, 68]. An important point to note in these studies is that XDM shows good performance in widely different systems without any change to the formalism, implementation, or damping parameters, hence making it an ideal candidate for studying chemistry on surfaces and the interaction between inorganic materials and organic molecules.

In the remainder of this paper, we show that XDM describes the graphene-nickel system accurately. Our results reproduce reported RPA potential energy surfaces[26, 42] and agree with available experimental adsorption energies.[69] We also show that the predicted mode of adsorption (chemisorption or physisorption) is highly sensitive to the nickel lattice constant, and that accounting for thermal effects favors the chemisorption state. The results are discussed in the

context of the mechanism of bilayer graphene formation on nickel substrates.

2. Computational Methods

Periodic-boundary DFT calculations were performed using the pseudopotential/plane-wave approach and the Projector Augmented Wave (PAW) formalism[70]. Calculations were carried out using the XDM implementation in Quantum ESPRESSO[46, 71] with the B86bPBE functional[72, 73], known to perform well in conjunction with XDM[61, 64]. Calculations using the LDA[74] and PBE[73] exchange-correlation functionals were also conducted for comparison. An $8 \times 8 \times 1$ Γ-centered **k**-point grid was used, with a plane-wave cutoff of 60 Ry, a density expansion cutoff of 800 Ry, and cold smearing[75] with a smearing parameter of 0.01 Ry.

The XDM dispersion functional is a correction to the base DFT energy:

$$E = E_{\text{base}} + E_{\text{XDM}} \tag{1}$$

$$E_{\text{XDM}} = -\frac{1}{2} \sum_{n=6,8,10} \sum_{i \neq j} \frac{C_{n,ij} f_n(R_{ij})}{R_{ij}^n} \tag{2}$$

In this equation, i and j run over atoms in the system and R_{ij} is the interatomic distance. f_n is a damping function that attenuates the dispersion correction at short range, and the $C_{n,ij}$ are pairwise dispersion coefficients. Each $C_{n,ij}$ is approximated non-empirically via second-order perturbation theory using the multipole moments of the electron plus exchange-hole distribution and atom-in-molecule polarizabilities for the interacting atoms.[39]

The nickel (111) surface was modeled as an infinite slab consisting of six atomic layers. All calculations used a (1×1) surface unit cell, with a vacuum of 25 Å inserted in the z-direction to separate each slab from its periodic image. Six orientations of graphene on nickel were considered for this study (see Figure 1). The adsorption energies were calculated as the difference between the graphene-nickel system and the energies of the bare surface and isolated graphene sheet, whose geometries were optimized independently:

$$E_{\text{adsorption}} = -\left(E_{\text{adsorbate}} - E_{\text{surf}} - E_{\text{graph}}\right) \tag{3}$$

Throughout the article, adsorption energies are reported per carbon atom.

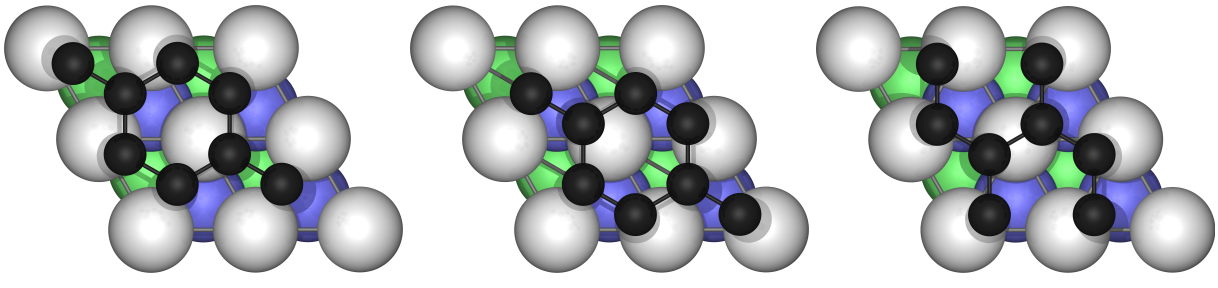

(a) bridge-fcc (b) bridge-hcp (c) bridge-top

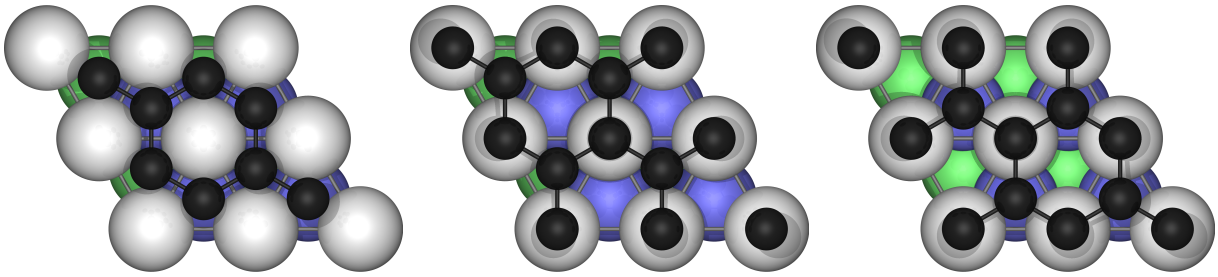

(d) fcc-hcp (e) top-fcc (f) top-hcp

Figure 1: Six orientations of graphene on nickel. The nickel top layer is shown in light gray, the second layer is blue, and the third layer from the surface is green. The nomenclature for the different graphene orientations follows previous works.[24, 32]

Potential energy surfaces (PES) for adsorption were generated by systematically varying the z distance between graphene and the nickel surface and performing a series of single-point energy calculations. The experimental lattice constants of graphene and nickel at room temperature are similar, but not exactly equal, and lattice vibrations cause a small, but not negligible, thermal expansion. As such, the dependence of the adsorption energy on the bulk lattice constant of the nickel slab was analysed. Note that this lattice constant defines the length of the two symmetry-equivalent x, y-axes for the nickel slab, and the nickel-nickel interlayer distances as well. Calculations were performed with the lattice constant ranging between 2.45 Å and 2.50 Å in 0.01 Å increments. This range encompasses the minimum-energy interatomic distances in bulk nickel (2.450 Å with B86bPBE-XDM and 2.451 Å with PBE-XDM) and in graphene (2.462 Å with both functionals), as well as the minimum-energy lattice constant of a pure nickel (111) surface (2.465 Å with B86bPBE-XDM and 2.464 Å with PBE-XDM). It also encompasses the experimental interatomic

distances in graphite (2.46 Å[76]), in bulk nickel (2.49 Å[76]), and in the nickel (111) surface (2.49 Å[77]). The final PES, minimum-energy structures, and adsorption energies for all orientations were obtained by quadratic interpolation between the results for each discrete value of the nickel lattice constant. This was done due to the strong dependence of the XDM dispersion coefficients on both the lattice constant and graphene-nickel separation (see the Supplementary Material).

Finally, The nature of the graphene-nickel interaction was investigated using Bader's Quantum Theory of Atoms in Molecules (QTAIM)[78, 79]. QTAIM atomic charges were calculated using the Yu-Trinkle algorithm[80] implemented in the CRITIC2 program[81]. The differences between the QTAIM charges for the isolated nickel and graphene sheet and the adsorbate determines the degree of charge transfer.

3. Results and Discussion

3.1. Orientation effects on adsorption

The computed B86bPBE-XDM interlayer separations and adsorption energies for all six graphene orientations are reported in Table 1. Reference distances taken from microscopy experiments[22, 82] are given for comparison. The reference adsorption energy range is reported as in the work of Janthon *et al.*[27] and is based on the energies for graphene-nickel adsorption[69] relative to the interlayer binding in graphite.[83, 84]

Figure 2 presents the calculated PES for adsorption of graphene in all six orientations, which clearly show the previously reported competing chemisorption and physisorption minima[26, 42]. The PES for all six orientations show a physisorption minimum at interlayer distances between 3.15 Å and 3.35 Å. However, only three of the six orientations exhibit a chemisorption minimum, consistent with previous DFT studies[24, 25, 32, 33]. The top-fcc orientation is found to be the most stable, in agreement with experimental observations[22, 33]. Both the chemisorption and physisorption energies fall well within the experimental range. The predicted interlayer distances for the chemisorbed geometries are also close to experiment, although slightly longer. The PES show that the energy barrier between the chemisorption and the physisorption regions is small, in

Table 1: Calculated B86bPBE-XDM interlayer distances and adsorption energies for all orientations of graphene on the nickel (111) surface at the minimum-energy nickel lattice constants. For the orientations in which chemisorption occurs, both the chemisorption (C) and the physisorption (P) values are given. Experimental distances[22, 82] and adsorption energies [27, 69] are shown for comparison. Distances are in Ångstrom (Å) and energies are in kJ/mol per carbon.

Orientation		Interlayer Distance	Adsorption Energy
bridge-fcc	P	3.25	8.00
bridge-hcp	P	3.26	7.97
fcc-hcp	P	3.34	7.54
bridge-top	C	2.14	7.31
	P	3.18	8.33
top-fcc	C	2.22	7.79
	P	3.15	8.50
top-hcp	C	2.28	6.48
	P	3.17	8.40
Expt.		2.04–2.18	7.20–11.20

agreement with previous RPA results[26, 42], and varies depending on the orientation. Although physisorption has not been experimentally observed for graphene on the nickel (111) surface, it has been observed in rotated Moiré patterns[23, 85, 86].

All orientations present essentially the same physisorption energy, which is in line with Olsen *et al.*'s RPA results[42]. Analysis of the separate base functional and XDM dispersion contributions to the adsorption potential energy surfaces (Supplementary Material) shows that the XDM dispersion energy is effectively independent of the graphene-nickel orientation. Thus, all variations in the shape of the PES for the various graphene orientations originate at the base functional level, from differences in both exchange-repulsion and charge-transfer between the surface and substrate.

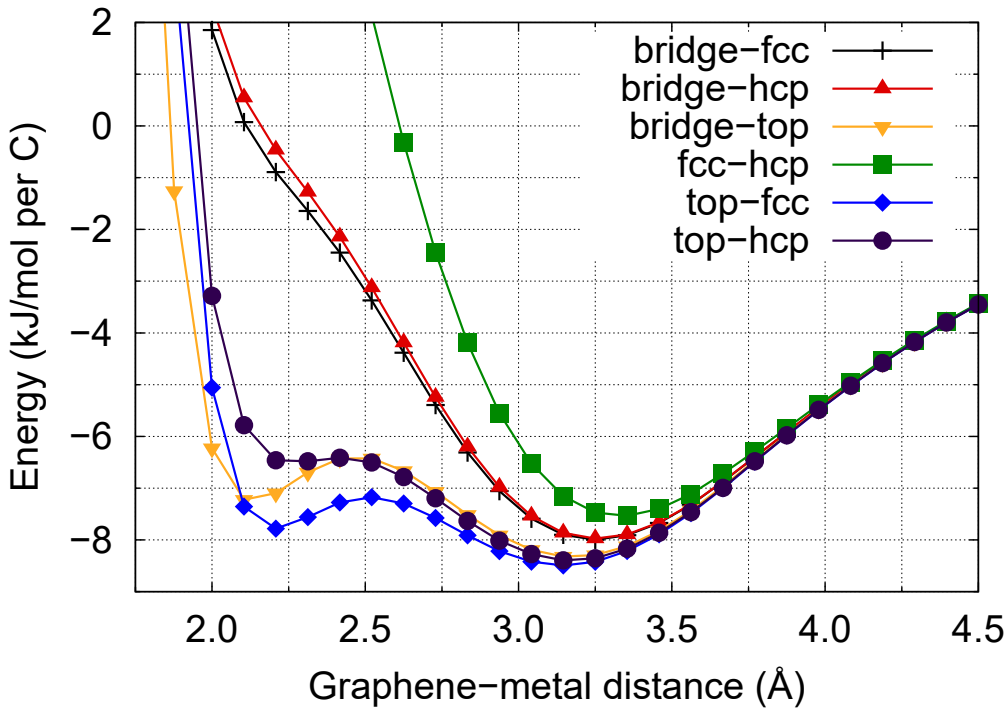

Figure 2: Adsorption energies as a function of interlayer distance for the six graphene-nickel orientations using the B86bPBE-XDM functional. At a given graphene-nickel distance the minimum-energy lattice constant is used.

The ordering of the adsorption energies for the different orientations can be understood by examining the interactions between the individual carbon and nickel atoms, as shown in Figure 1. For the physisorption minima, the bridge-fcc and bridge-hcp orientations show slightly stronger adsorption than fcc-hcp because there is slight, though significant, carbon-nickel overlap. At shorter interlayer distances, these three orientations (bridge-fcc, bridge-hcp, and fcc-hcp) all show a steep repulsive wall whereas the other three (top-fcc, top-hcp, and bridge-top) show the formation of a chemisorption energy minimum. In the chemisorbed orientations, one carbon is either directly on top of a nickel atom (top-fcc and top-hcp) or two carbons straddle a single nickel (bridge-top), which is indicative of a weak chemical bond between both layers. The sub-surface nickel atoms lie directly under the second carbon atom in the top-hcp orientation, which provides less stabilization than if the sub-surface nickel atoms lie below the center of each graphene ring, as in the top-fcc orientation. The bridge-top orientation has a shorter interlayer separation despite its lower adsorption energy because the two carbon atoms bridge two nickel atoms, allowing the graphene

to approach the surface more closely.

The small energy barrier between chemisorption and physisorption minima for the most-stable, top-fcc orietation suggests that physisorbed states may be accessible through thermal fluctuations[85]. It also may provide insight into graphene bilayer formation mechanisms. A graphene bilayer forms from the creation of a new graphene layer under an existing nickel-adsorbed graphene layer[18, 25, 85]. The proposed mechanism is based on nickel's carbon solubility during CVD[18, 25, 85]. Upon cooling, the carbon atoms exit the bulk, but are trapped beneath the existing chemisorbed graphene monolayer. The carbon atoms must push up the adsorbed graphene to assemble at the nickel surface and form a second underlying layer of graphene. The presence of a small energy barrier between the chemisorbed and physisorbed minima means that it would take little energy to displace an existing graphene monolayer, allowing for the facile accumulation and migration of carbon on the surface necessary to the formation of the graphene bilayer.

3.2. Comparison of selected desnity functionals

Calculated adsorption energies as a function of interlayer distance for the top-fcc using B86bPBE-XDM, PBE-XDM, and the LDA are compared with reference RPA values[26, 42] in Figure 3. For the XDM-corrected functionals, two sets of potential-energy curves are shown, using either the minimum-energy nickel lattice constant (as in Figure 2) or using the experimental nickel lattice constant to allow direct comparison with the RPA results.

Figure 3 shows remarkable agreement between the minimum-energy B86bPBE-XDM potential-energy surface and experiment; the chemisorption energy is in the experimental energy range, and the distance is only 0.04 Å higher. Additionally, the equilibrium distances and absorption energies at the experimental nickel lattice constant are in good agreement with the analogous RPA calculations[26, 42]. The B86bPBE-XDM chemisorption and physiorption energies are within 1 kJ/mol and 0.5 kJ/mol, respectively, from the RPA equivalents. Interlayer distances are also in excellent agreement with RPA. PBE-XDM provides similar potential energy surfaces to B86bPBE-XDM, although the PBE-XDM curves are slightly higher in energy and also have higher energy barriers between the chemisorbed and physisorbed minima.

It has been suggested that accurate modeling of surface adsorption can only be achieved

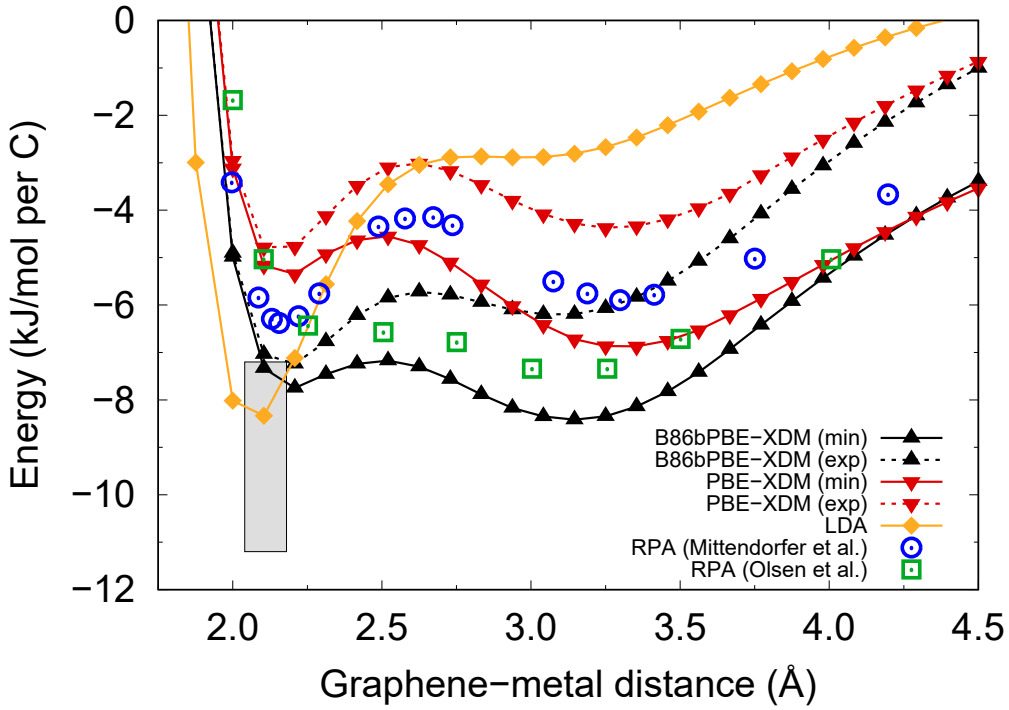

Figure 3: Adsorption energies as a function of interlayer distance for the top-fcc orientation using the B86bPBE-XDM (black), PBE-XDM (red), and LDA (orange) functionals. The RPA results digitized from the work by Mittendorfer *et al.*[26] (blue circles) and by Olsen *et al.*[42] (green squares) are also shown. The experimental distance and energy ranges are shown as a shaded box[22, 27, 69, 82]. For B86bPBE-XDM and PBE-XDM, two results are shown: energies using a minimum-energy lattice constant (solid lines) and the experimental bulk nickel lattice constant (dashed lines).

through use of many-body dispersion corrections and not with "simple pair-wise" methods[87–90]. A significant advantage of the XDM dispersion model over simple pair-wise methods is that the dispersion coefficients are sensitive to the chemical environment in a physically-motivated way and this dependence was key to the high accuracy of the method in studies of molecular physisorption on noble metal surfaces.[67] In the present study, the surface nickel-carbon C_6 dispersion coefficients were found to exhibit a strong dependence on both the interlayer separation and the lattice constant (see the Supplementary Material). In particular, these C_6's decrease substantially as graphene approaches the nickel surface, due to a decrease in the exchange-hole dipole moment integral caused by compaction of the interface region between the graphene and the nickel surface. This behaviour is only seen for nickel atoms at or near the surface; beyond the top two layers, there

is no longer any change in the dispersion coefficients upon graphene adsorption. It is clear from the good agreement between the B86bPBE-XDM results and both RPA and experimental data that environmental effects captured by XDM's use of the self-consitent ground-state electron density are at least as important as non-pairwise many-body effects when modeling dispersion.

Comparison with literature adsorption energies and interlayer distances for the other orientations is included in the Supplementary Material. B86bPBE-XDM and PBE-XDM both predict chemisorption for the bridge-top and top-fcc orientations and physisorption at the fcc-hcp orientation. These are two of the three criteria for by Janthon *et al.*[27] for accurate modeling of graphene-nickel interactions. The third criterion proposed by these authors is that graphene-nickel adsorption energies must be greater than the exfoliation energy of graphite, which is also met by B86bPBE-XDM (5.27 kJ/mol[46]) and PBE-XDM (4.76 kJ/mol[46]). These values are in good agreement with RPA's graphite exfoliation energy (4.63 kJ/mol[26]), as well as the reference experimental value (5.07 kJ/mol[83]).

Finally, although the LDA predicts a chemisorption energy and interlayer distance in good agreement with experiment, the chemisorption energy is less than the calculated LDA graphite exfoliation energy (2.39 kJ/mol[26]), in violation of the last of Janthon's criteria. Figure 3 shows that the LDA potential-energy surface is quite different than the DFT-XDM or RPA curves. The LDA physisorption minimum is very shallow and lies much higher in energy, due to the neglect of long-range dispersion stabilization. Thus, while the LDA predicts adequate adsorption energies and interlayer distances for chemisorption, the failure to correctly describe physisorption means that LDA cannot be recommended for any applications involving surface chemistry.

3.3. Lattice effects on adsorption

Our calculations reveal a strong dependence of the calculated chemisorption and physisorption energies on the nickel lattice constant. The optimum lattice constant for the graphene monolayer is predicted to be 2.46 Å with B86bPBE-XDM which is the same as seen in experiment[91]. However, there is notable difference between theory and experiment for the nickel lattice constant. The energy minimum for the bare nickel surface was found to occur at a lattice constant equal to 2.465 Å for B86bPBE-XDM (as well as PBE-XDM), which is smaller than the experimental value

of 2.49 Å[77]. This underestimation of the nickel lattice constant is characteristic for relatively soft materials, and occurs due to neglect of vibrational and other thermal-expansion effects. These are more significant in nickel than graphene because of the more compressible nature of the nickel surface.

Figure 4 illustrates how small changes in the lattice constant affect the graphene-nickel potential energy surface. At the smallest tested lattice parameter, there is no chemisorption and only a physisorption minimum. Increasing the lattice constant lowers the repulsive shoulder significantly and the chemisorption minimum appears. The strongest physisorption occurs for lattice constants 2.46–2.47 Å which corresponds to the graphene lattice constant. However, the strongest chemisorption occurs when the lattice constant is equal to 2.48 Å. At this lattice constant, the C-C bonds are slightly stretched from 1.421 Å to 1.432 Å, but the energy penalty incurred in this process is offset by the much stronger C-Ni interactions. Thus, the physisorption minimum is destabilized and the chemisorption minimum stabilized as the lattice-constant approaches the experimental nickel lattice constant of 2.49 Å[77].

Figure 5 is a two dimensional potential energy surface that shows how the top-fcc adsorption energy changes as a function of lattice constant and interlayer distance. The chemisorption minimum begins to stabilize at 2.46 Å and is competitive with the physisorption minimum near 2.47 Å. At 2.48 Å, the physisorption is destabilized and the chemisorption minimum becomes the more stable region of the potential. Above 2.50 Å, the entire system destabilizes due to the highly stretched C-C bonds. Generally, the physisorbed configuration is preferred when the lattice constant is closer to the experimental graphene lattice constant and the chemisorption configuration is preferred as the lattice constant approaches the experimental nickel lattice constant.

The important result coming from Figures 4 and 5 is that, for all lattice surface constants above a given threshold value (ca. 2.48 Å), the chemisorption minimum is more stable than the physisorption minimum. The simple but reasonable assumption can be made that the adsorption free energy is given by Figure 5, after adjusting the geometry for the effects of thermal expansion. This approximation is equivalent to a combination of a quasi-harmonic approach and a neglect of the differences in the free-energy contributions as a function of temperature, which we expect to be smaller than the differences in electronic energies. Under this assumption, our data predicts that

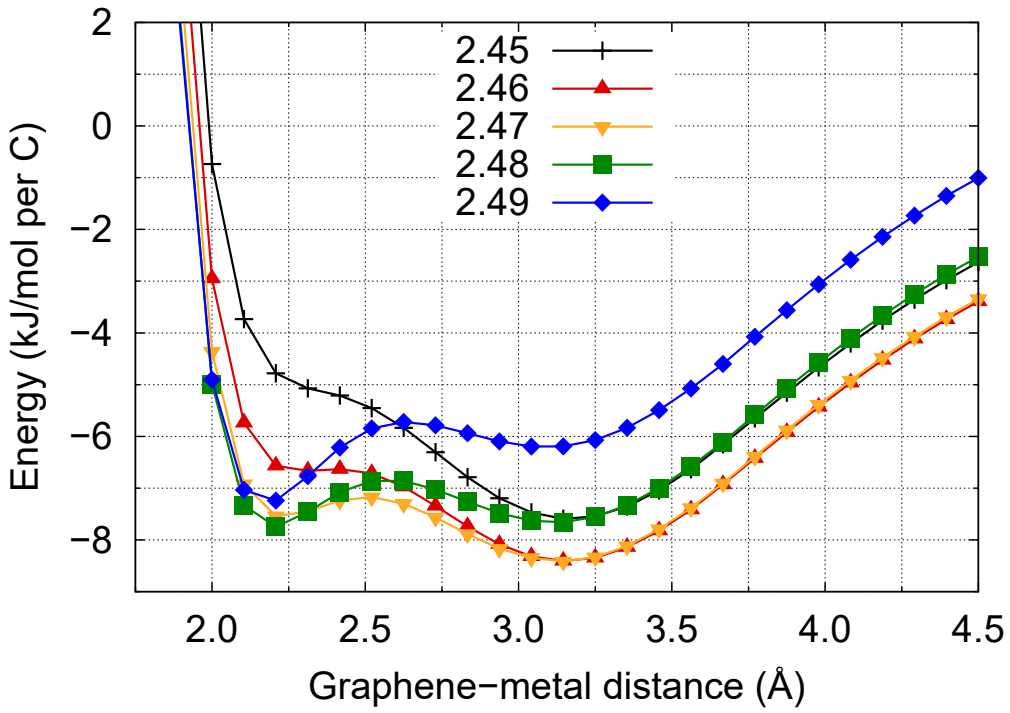

Figure 4: The B86bPBE-XDM potential energy surface for the top-fcc graphene-nickel orientation for lattice constants ranging from 2.45 Å to 2.49 Å.

chemisorption is favored compared to physisorption at the experimental geometry, in agreement with the experimental observations. We therefore expect chemisorption to be somewhat preferred over physisorption if thermal expansion of the nickel surface were taken into account in our calculations. In addition, we also predict that a decrease in temperature may eventually result in a physisorbed state, although the zero-point vibrational contribution to thermal expansion may already send the system over the threshold at 0 K.

3.4. Charge Transfer

Analysis of the charge transfer between nickel and graphene is presented in Table 2. This table reports the atomic charges for the three chemisorbed geometries at the experimental lattice constant for nickel (2.49 Å). The charge transfer for all of the physisorbed structures is zero, and is not shown. The largest charge transfer from nickel to graphene occurs for the bridge-top orientation since both carbon atoms in the periodic cell bridge the surface nickel atoms equally,

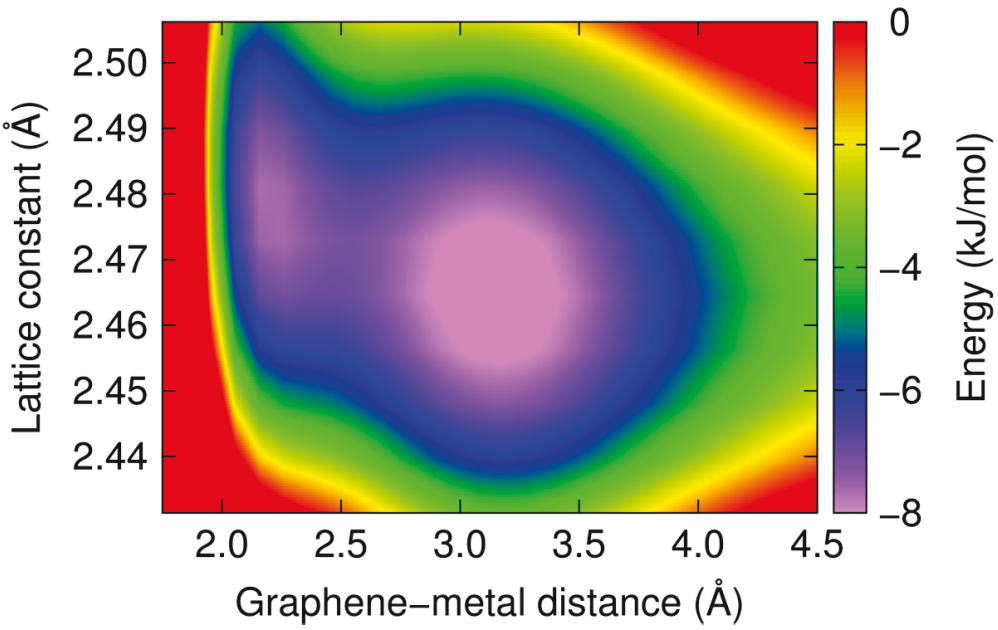

Figure 5: Two-dimensional B86bPBE-XDM potential energy surface, illustrating the dependence of the adsorption energy for the top-fcc graphene-nickel orientation on the lattice constant.

leading to the shortest interlayer separation. The top-fcc and top-hcp orientations have similar interlayer distances, but the top-fcc has a stronger adsorption energy and higher charge transfer.

Table 2 also shows that charge transfer from the graphene to the nickel surface increases as lattice constant increases for the top-fcc orientation. The charge transfer from nickel to graphene correlates with the optimum graphene-nickel distance for the chemisorption minimum of the PES shown in Figure 1. Experimentally, it has been confirmed that graphene carbon-carbon bonds expand upon chemisorption, distorting the structure such that the graphene lattice constant becomes commensurate with that of nickel[22, 25, 77]. Spectroscopic measurements have shown that graphene's band structure is strongly perturbed upon adsorption[91–93]. Taken together with our results, this provides evidence that charge transfer is related to the stabilizion of the deformed graphene layer[25].

Table 2: Charge of the two unique carbon atoms in the (1×1) cell and the surface nickel atom obtained from QTAIM analysis of the B86bPBE electron densities. Results are shown for the three chemisorbed orientations at a lattice constant of 2.49 Å and for the top-fcc orientation with lattice constants ranging from 2.46 to 2.49 Å. In all cases except bridge-top, C_{top} represents the carbon directly above a nickel atom.

	Ni	C_{top}	C_{other}
bridge-top	0.084	-0.049	-0.050
top-fcc	0.082	-0.069	-0.028
top-hcp	0.080	-0.069	-0.027
2.46	0.077	-0.067	-0.028
2.47	0.079	-0.067	-0.028
2.48	0.080	-0.068	-0.028
2.49	0.082	-0.069	-0.028

4. Summary

This paper presented a detailed density-functional study of graphene adsorption on the nickel (111) surface. Our results show that both the B86bPBE-XDM and PBE-XDM methods predict optimum interlayer distances and adsorption energies in excellent agreement with previously reported reference RPA results[26, 42] and available experimental data.[22, 27, 69, 82] Thus, surface adsorption can be accurately modeled by a pair-wise atomic dispersion correction provided that the dispersion coefficients have an appropriate dependence on the chemical environment.

Graphene was found to physisorb to the nickel surface in all six graphene orientations considered (see Figure 1), at a distance between 3.15 and 3.35 Å. The physisorption energies increase slightly with the number of close carbon-nickel atomic contacts. In this state, there is no significant chemical bond between graphene and nickel, and the binding is determined by dispersion plus closed-shell repulsion between both surfaces.

Three of the studied orientations (bridge-top, top-fcc and top-hcp) have chemisorption minimum with optimum graphene-metal distances between 2.00 and 2.25 Å. The top-fcc orienta-

tion was found to be the most stable, in agreement with previous theoretical studies[22, 24, 25, 32, 33, 82]. The potential energy as a function of interlayer distance for these orientations is a double-minimum curve, with the barrier between the physisorption and chemisorption minima being less than 1 kJ/mol per carbon. This suggests that physisorbed states may be accessible through thermal fluctuations[85], and offers insight into the double-layer graphene formation in CVD experiments[18, 25, 85]. Both the chemisorption and physisorption energies are higher than the calculated graphite exfoliation energies.

The B86bPBE-XDM chemisorption energies are in the experimental energy range[27, 69] and they also agree with RPA results[26] to within 1 kJ/mol (chemisorption) and 0.5 kJ/mol (physisorption) per carbon when the same lattice constant is used. We note, however, that the precision of the experimental data is 4 kJ/mol, and the two previously reported RPA potential energy surfaces are somewhat in disagreement with each other (up to about 2 kJ/mol), specifically regarding the presence of a double minimum in the energy profile. Hence, higher-quality reference data is required before the accuracy of B86bPBE-XDM can be precisely quantified.

In the chemisorbed state, there is significant charge transfer between graphene and nickel, which increases with the lattice constant. This is indicative of the formation of a weak chemical bond and the disruption of the nickel and graphene band structures, as previously observed[41, 91–93]. The differences in the chemisorption behavior between orientations are determined by whether there is a direct carbon-nickel contact that facilitates the approach between both surfaces. Therefore, it is the base functional contribution, and not the dispersion correction, that determines the behavior in the chemisorption distance range, although the dispersion correction is a major component of the adsorption energy in all orientations.

It was also found that the graphene-nickel adsorption is strongly dependent on the lattice geometry, which somewhat hinders the comparison to experimental results. At the electronic energy minimum (lattice constant around 2.46 Å), physisorption is preferred over chemisorption. However, as the lattice constant increases, chemisorption becomes the preferred state at a surface lattice constant equal to 2.48 Å. Thermal expansion pushes the lattice constant over this threshold (the experimental lattice constant is 2.49 Å for the nickel (111) surface), resulting in a stabilization of the experimentally-observed chemisorption state.

Acknowledgement: We are grateful for financial support from the Natural Sciences and Engineering Research Council (NSERC), and for computational resources and support from ACEnet, Westgrid and Compute Canada/Calcul Canada.

[1] K. S. Novoselov, A. K. Geim, S. Morozov, D. Jiang, Y. Zhang, S. Dubonos, I. Grigorieva, A. A. Firsov, Electric field effect in atomically thin carbon films., Science 306 (2004) 666.

[2] A. H. Castro-Neto, F. Guinea, N. M. R. Peres, K. S. Novoselov, A. K. Geim, The electronic properties of graphene, Rev. Mod. Phys. 81 (2009) 109.

[3] A. K. Geim, K. S. Novoselov, The rise of graphene, Nat. Mater. 6 (2007) 183.

[4] P. Plachinda, D. R. Evans, R. Solanki, Electronic properties of metal-arene functionalized graphene, J. Chem. Phys. 135 (2011) 044103. doi:10.1063/1.3613649.

[5] S. Das Sarma, S. Adam, E. H. Hwang, E. Rossi, Electronic transport in two-dimensional graphene, Rev. Mod. Phys. 83 (2011) 407.

[6] V. Singh, D. Joung, L. Zhai, S. Das, S. I. Khondaker, S. Seal, Graphene based materials: Past, present and future, Prog. Mater. Sci. 56 (2011) 1178.

[7] S. Guo, S. Dong, Graphene nanosheet: synthesis, molecular engineering, thin film, hybrids, and energy and analytical applications, Chem. Soc. Rev. 40 (2011) 2644.

[8] Z. Xu, Q. Zhang, X. Shi, W. Zhai, Q. Zhu, Comparison of Tribological Properties of NiAl Matrix Composites Containing Graphite, Carbon Nanotubes, or Graphene, J. Mater. Eng. Perform. 24 (2015) 1926.

[9] M. S. Won, O. V. Penkov, D. E. Kim, Durability and degradation mechanism of graphene coatings deposited on Cu substrates under dry contact sliding, Carbon N. Y. 54 (2013) 472.

[10] H. Chen, T. Filleter, Effect of structure on the tribology of ultrathin graphene and graphene oxide films, Nanotechnology 26 (2015) 135702. doi:10.1088/0957-4484/26/13/135702.

[11] D. Berman, S. A. Deshmukh, S. K. Sankaranarayanan, A. Erdemir, A. V. Sumant, Extraordinary Macroscale Wear Resistance of One Atom Thick Graphene Layer, Adv. Funct. Mater. 24 (2014) 6640–6646. doi:10.1002/adfm.201401755.

[12] S. Cahangirov, S. Ciraci, V. O. Özçelik, Superlubricity through graphene multilayers between Ni(111) surfaces, Phys. Rev. B - Condens. Matter Mater. Phys. 87 (2013) 1. doi:10.1103/PhysRevB.87.205428.

[13] M. Tripathi, F. Awaja, G. Paolicelli, R. Bartali, E. Iacob, S. Valeri, S. Ryu, S. Signetti, G. Speranza, N. M. Pugno, Tribological characteristics of few-layer graphene over ni grain and interface boundaries, Nanoscale 8 (2016) 6646–6658. doi:10.1039/c5nr06273j.

[14] O. Penkov, H. J. Kim, H. J. Kim, D. E. Kim, Tribology of graphene: A review, Int. J. Precis. Eng. Manuf. 15 (2014) 577. doi:10.1007/s12541-014-0373-2.

[15] L. Zhao, K. T. Rim, H. Zhou, R. He, T. F. Heinz, A. Pinczuk, G. W. Flynn, A. N. Pasupathy, Influence of copper crystal surface on the CVD growth of large area monolayer graphene, Solid State Commun. 151 (2011) 509.

[16] R. Muñoz, C. Gómez-Aleixandre, Review of CVD synthesis of graphene, Chem. Vap. Depos. 19 (2013) 297.

[17] J. Coraux, A. T. N'Diaye, M. Engler, C. Busse, D. Wall, N. Buckanie, F. J. Meyer Zu Heringdorf, R. Van Gastel, B. Poelsema, T. Michely, Growth of graphene on Ir(111), New J. Phys. 11 (2009) 565. doi:10.1088/1367-2630/11/2/023006.

[18] N. Bartelt, K. McCarty, Graphene growth on metal surfaces, MRS Bull. 37 (2012) 1158.

[19] M. Batzill, The surface science of graphene: Metal interfaces, CVD synthesis, nanoribbons, chemical modifications, and defects, Surf. Sci. Rep. 67 (2012) 83. doi:10.1016/j.surfrep.2011.12.001.

[20] H. J. Park, J. Meyer, S. Roth, V. Skákalová, Growth and properties of few-layer graphene prepared by chemical vapor deposition, Carbon N. Y. 48 (2010) 1088.

[21] Y. Zhang, L. Zhang, C. Zhou, Review of chemical vapor deposition of graphene and related applications, Acc. Chem. Res. 46 (2013) 2329. doi:10.1021/ar300203n.

[22] Y. Gamo, A. Nagashima, M. Wakabayashi, M. Terai, C. Oshima, Atomic Structure of Monolayer Graphite Formed on Ni(111), Hyomen Kagaku 17 (1996) 745. doi:10.1380/jsssj.17.745.

[23] Y. Zhang, T. Gao, S. Xie, B. Dai, L. Fu, Y. Gao, Y. Chen, M. Liu, Z. Liu, Different growth behaviors of ambient pressure chemical vapor deposition graphene on Ni(111) and Ni films: A scanning tunneling microscopy study, Nano Res. 5 (2012) 402. doi:10.1007/s12274-012-0221-6.

[24] W. Zhao, S. M. Kozlov, H. Oliver, K. Gotterbarm, M. P. A. Lorenz, F. Viñes, C. Papp, G. Andreas, H.-P. Steinrück, Graphene on Ni (111): Coexistence of Different Surface Structures, J. Chem. Phys. Lett. 2 (2011) 759. doi:10.1021/jz200043p.

[25] A. Dahal, M. Batzill, Graphenenickel interfaces: a review, Nanoscale 6 (2014) 2548. doi:10.1039/c3nr05279f.

[26] F. Mittendorfer, A. Garhofer, J. Redinger, J. Klimeš, J. Harl, G. Kresse, Graphene on Ni(111): Strong interaction and weak adsorption, Phys. Rev. B - Condens. Matter Mater. Phys. 84 (2011) 2. doi:10.1103/PhysRevB.84.201401.

[27] P. Janthon, F. Viñes, S. M. Kozlov, J. Limtrakul, F. Illas, Theoretical assessment of graphene-metal contacts, J. Chem. Phys. 138 (2013) 244701. doi:10.1063/1.4807855.

[28] M. Vanin, J. Mortensen, A. Kelkkanen, J. Garcia-Lastra, K. Thygesen, K. Jacobsen, Graphene on metals: A van der Waals density functional study, Phys. Rev. B 81 (2010) 081408. doi:10.1103/PhysRevB.81.081408.

[29] C. Gong, G. Lee, B. Shan, E. M. Vogel, R. M. Wallace, K. Cho, First-principles study of metal-graphene interfaces, J. Appl. Phys. 108 (2010) 123711. doi:10.1063/1.3524232.

[30] I. Hamada, M. Otani, Comparative van der Waals density-functional study of graphene on metal surfaces, Phys. Rev. B 82 (2010) 153412. doi:10.1103/PhysRevB.82.153412.

[31] P. A. Khomyakov, G. Giovannetti, P. C. Rusu, G. Brocks, J. Van Den Brink, P. J. Kelly, First-principles study of

the interaction and charge transfer between graphene and metals, Phys. Rev. B - Condens. Matter Mater. Phys. 79 (2009) 1.

[32] W. B. Zhang, C. Chen, P. Y. Tang, First-principles study for stability and binding mechanism of graphene/Ni(111) interface: Role of vdW interaction, J. Chem. Phys. 141. doi:10.1063/1.4890728.

[33] F. Bianchini, L. L. Patera, M. Peressi, C. Africh, G. Comelli, Atomic Scale Identification of Coexisting Graphene Structures on Ni(111), J. Chem. Phys. Lett. 5 (2014) 467–473.

[34] G. A. DiLabio, A. Otero-de-la Roza, Noncovalent Interactions in Density Functional Theory, Vol. 29, John Wiley & Sons, Inc, 2016, pp. 1–97. doi:10.1002/9781119148739.ch1.

[35] E. R. Johnson, I. D. Mackie, G. A. DiLabio, Dispersion interactions in density-functional theory, J. Phys. Org. Chem. 22 (2009) 1127–1135. doi:10.1002/poc.1606.

[36] S. Grimme, Density functional theory with london dispersion corrections, Wiley Interdisciplinary Reviews: Computational Molecular Science 1 (2011) 211–228.

[37] A. Tkatchenko, M. Scheffler, Accurate molecular van der waals interactions from ground-state electron density and free-atom reference data, Phys. Rev. Lett. 102 (2009) 073005. doi:10.1103/PhysRevLett.102.073005.

[38] S. Grimme, J. Antony, S. Ehrlich, H. Krieg, A consistent and accurate ab initio parametrization of density functional dispersion correction (dft-d) for the 94 elements h-pu, J. Chem. Phys. 132 (2010) 154104.

[39] A. D. Becke, E. R. Johnson, Exchange-hole dipole moment and the dispersion interaction revisited, J. Chem. Phys. 127 (15) (2007) 154108.

[40] H. Kawanowa, H. Ozawa, T. Yazaki, Y. Gotoh, R. Souda, Structure analysis of monolayer graphite on ni (111) surface by li+-impact collision ion scattering spectroscopy, Japanese journal of applied physics 41 (2002) 6149.

[41] S. M. Kozlov, F. Vines, A. Gorling, Bonding mechanisms of graphene on metal surfaces, J. Phys. Chem. C 116 (2012) 7360–7366.

[42] T. Olsen, J. Yan, J. J. Mortensen, K. S. Thygesen, Dispersive and covalent interactions between graphene and metal surfaces from the random phase approximation, Physical review letters 107 (2011) 156401.

[43] M. Dion, H. Rydberg, E. Schröder, D. C. Langreth, B. I. Lundqvist, Van der Waals density functional for general geometries, Phys. Rev. Lett. 92 (2004) 246401. doi:10.1103/PhysRevLett.92.246401.

[44] T. Thonhauser, V. Cooper, S. Li, A. Puzder, P. Hyldgaard, D. Langreth, Van der waals density functional: Self-consistent potential and the nature of the van der waals bond, Phys. Rev. B 76 (2007) 125112.

[45] D. Langreth, B. I. Lundqvist, S. D. Chakarova-Käck, V. Cooper, M. Dion, P. Hyldgaard, A. Kelkkanen, J. Kleis, L. Kong, S. Li, P. G. Moses, E. Murray, A. Pudzer, H. Rydberg, E. Schröder, T. Thonhauser, A density functional for sparse matter, J. Phys.: Condens. Matter 21 (2009) 084203.

[46] A. Otero-de-la-Roza, E. R. Johnson, Van der waals interactions in solids using the exchange-hole dipole moment, J. Chem. Phys. 136 (2012) 174109.

[47] S. Grimme, Accurate description of van der Waals complexes by density functional theory including empirical

corrections, J. Comput. Chem. 25 (2004) 1463. doi:10.1002/jcc.20078.

[48] S. Grimme, Semiempirical gga-type density functional constructed with a long-range dispersion correction, J. Comput. Chem. 27 (2006) 1787–1799.

[49] V. G. Ruiz, W. Liu, E. Zojer, M. Scheffler, A. Tkatchenko, Density-functional theory with screened van der Waals interactions for the modeling of hybrid inorganic-organic systems, Phys. Rev. Lett. 108 (2012) 2. doi:10.1103/PhysRevLett.108.146103.

[50] J. c. v. Klimeš, D. R. Bowler, A. Michaelides, Van der waals density functionals applied to solids, Phys. Rev. B 83 (2011) 195131. doi:10.1103/PhysRevB.83.195131.

[51] K. Tonigold, A. Gross, Adsorption of small aromatic molecules on the (111) surfaces of noble metals: A density functional theory study with semiempirical corrections for dispersion effects, J. Chem. Phys. 132 (2010) 224701.

[52] J. Carrasco, W. Liu, A. Michaelides, A. Tkatchenko, Insight into the description of van der waals forces for benzene adsorption on transition metal (111) surfaces, J. Chem. Phys. 140 (2014) 084704.

[53] W. Liu, V. G. Ruiz, G.-X. Zhang, B. Santra, X. Ren, M. Scheffler, A. Tkatchenko, Structure and energetics of benzene adsorbed on transition-metal surfaces: density-functional theory with van der waals interactions including collective substrate response, New J. Phys. 15 (5) (2013) 053046.

[54] H. Muñoz-Galán, F. Viñes, J. Gebhardt, A. Görling, F. Illas, The contact of graphene with ni (111) surface: description by modern dispersive forces approaches, Theor. Chem. Acc. 135 (2016) 1–9.

[55] A. D. Becke, E. R. Johnson, Exchange-hole dipole moment and the dispersion interaction, J. Chem. Phys. 122 (15) (2005) 154104.

[56] A. D. Becke, E. R. Johnson, Exchange-hole dipole moment and the dispersion interaction: High-order dispersion coefficients, J. Chem. Phys. 124 (2006) 014104.

[57] A. Otero-de-la-Roza, E. R. Johnson, Many-body dispersion interactions from the exchange-hole dipole moment model, J. Chem. Phys. 138 (2013) 054103.

[58] F. O. Kannemann, A. D. Becke, Van der waals interactions in density-functional theory: Rare-gas diatomics, J. Chem. Theory Comput. 5 (4) (2009) 719–727.

[59] J. B. Dizon, E. R. Johnson, van der waals potential energy surfaces from the exchange-hole dipole moment dispersion model, Can. J. Chem. 94 (2016) 1049–1056.

[60] F. Kannemann, A. Becke, van der waals interactions in density-functional theory: Intermolecular complexes, J. Chem. Theory Comput. 6 (2010) 1081–1088.

[61] A. Otero-de-la-Roza, E. R. Johnson, Non-covalent interactions and thermochemistry using xdm-corrected hybrid and range-separated hybrid density functionals, J. Chem. Phys. 138 (20) (2013) 054103.

[62] A. Otero-de-la-Roza, J. D. Mallory, E. R. Johnson, Metallophilic interactions from dispersion-corrected density-functional theory, J. Chem. Phys. 140 (2014) 18A504.

[63] A. Otero-de-la-Roza, E. R. Johnson, Predicting Energetics of Supramolecular Systems Using the XDM Disper-

sion Model, J. Chem. Theory Comput. 11 (2015) 4033. doi:10.1021/acs.jctc.5b00044.

[64] A. Otero-de-la-Roza, E. R. Johnson, A benchmark for non-covalent interactions in solids, J. Chem. Phys. 137 (2012) 054103.

[65] A. Otero-de-la-Roza, B. H. Cao, I. K. Price, J. E. Hein, E. R. Johnson, Predicting the relative solubilities of racemic and enantiopure crystals by density-functional theory, Angew. Chem. Int. Ed. 53 (2014) 7879–7882. doi:10.1002/anie.201403541.

[66] S. Whittleton, A. Otero-de-la-Roza, E. R. Johnson, Molecular crystal polymorphism using the exchange-hole dipole moment dispersion model, J. Chem. Theory Comput.(published online). doi:10.1021/acs.jctc.6b00679.

[67] M. S. Christian, A. Otero-De-La-Roza, E. R. Johnson, Surface adsorption from the exchange-hole dipole moment dispersion model, J. Chem. Theory Comput. 12 (2016) 3305. doi:10.1021/acs.jctc.6b00222.

[68] E. R. Johnson, A. Otero-de-la-Roza, Adsorption of organic molecules on kaolinite from the exchange-hole dipole moment dispersion model, J. Chem. Theory Comput. 8 (2012) 5124–5131. doi:10.1021/ct3006375.

[69] J. Shelton, H. Patil, J. Blakely, Equilibrium segregation of carbon to a nickel (111) surface: A surface phase transition, Surf. Sci. 43 (1974) 493.

[70] P. E. Blöchl, Projector augmented-wave method, Phys. Rev. B 50 (24) (1994) 17953.

[71] P. Giannozzi, S. Baroni, et. al., Quantum espresso: a modular and open-source software project for quantum simulations of materials, J. Phys. Condens. Mat. 21 (39) (2009) 395502.

[72] A. D. Becke, On the large-gradient behavior of the density functional exchange energy, J. Chem. Phys. 85 (1986) 7184.

[73] J. P. Perdew, K. Burke, M. Ernzerhof, Generalized gradient approximation made simple, Phys. Rev. Lett. 77 (18) (1996) 3865.

[74] J. P. Perdew, A. Zunger, Self-interaction correction to density-functional approximations for many-electron systems, Phys. Rev. B 23 (1981) 5048. doi:10.1103/PhysRevB.23.5048.

[75] N. Marzari, D. Vanderbilt, A. De Vita, M. C. Payne, Thermal contraction and disordering of the Al(110) surface, Phys. Rev. Lett. 82 (1999) 3296.

[76] R. Wyckoff, Crystal structures, Interscience publishers, New York, 1960.

[77] L. V. Dzemiantsova, M. Karolak, F. Lofink, A. Kubetzka, B. Sachs, K. Von Bergmann, S. Hankemeier, T. O. Wehling, R. Frömter, H. P. Oepen, A. I. Lichtenstein, R. Wiesendanger, Multiscale magnetic study of Ni(111) and graphene on Ni(111), Phys. Rev. B - Condens. Matter Mater. Phys. 84 (2011) 1. doi:10.1103/PhysRevB.84.205431.

[78] R. F. W. Bader, Atoms in Molecules. A Quantum Theory, Oxford University Press, Oxford, 1990.

[79] R. F. W. Bader, A quantum theory of molecular structure and its applications, Chem. Rev. 91 (1991) 893.

[80] M. Yu, D. R. Trinkle, Accurate and efficient algorithm for Bader charge integration, J. Chem. Phys. 134 (2011) 064111. doi:10.1063/1.3553716.

[81] A. Otero-de-la-Roza, E. R. Johnson, V. Luaña, Critic2: A program for real-space analysis of quantum chemical interactions in solids, Comput. Phys. Commun. 185 (3) (2014) 1007.

[82] J. Sun, J. B. Hannon, R. M. Tromp, P. Johari, A. A. Bol, V. B. Shenoy, K. Pohl, Spatially-resolved structure and electronic properties of graphene on polycrystalline Ni, ACS Nano 4 (2010) 7073. doi:10.1021/nn102167f.

[83] R. Zacharia, H. Ulbricht, T. Hertel, Interlayer cohesive energy of graphite from thermal desorption of polyaromatic hydrocarbons, Phys. Rev. B - Condens. Matter Mater. Phys. 69 (2004) 1. doi:10.1103/PhysRevB.69.155406.

[84] L. X. Benedict, N. G. Chopra, M. L. Cohen, A. Zettl, S. G. Louie, V. H. Crespi, Microscopic determination of the interlayer binding energy in graphite, Chem. Phys. Lett. 286 (1998) 490. doi:10.1016/S0009-2614(97)01466-8.

[85] A. Dahal, R. Addou, P. Sutter, M. Batzill, Graphene monolayer rotation on Ni(111) facilitates bilayer graphene growth, Appl. Phys. Lett. 100 (2012) 241602. doi:10.1063/1.4729150.

[86] P. Zeller, F. Speck, M. Weinl, M. Ostler, M. Schreck, T. Seyller, J. Wintterlin, Healing of graphene on single crystalline Ni(111) films, Appl. Phys. Lett. 105 (2014) 2012. doi:10.1063/1.4902057.

[87] R. J. Maurer, V. G. Ruiz, A. Tkatchenko, Many-body dispersion effects in the binding of adsorbates on metal surfaces, J. Chem. Phys. 143 (2015) 102808.

[88] W. Liu, F. Maaß, M. Willenbockel, C. Bronner, M. Schulze, S. Soubatch, F. S. Tautz, P. Tegeder, A. Tkatchenko, Quantitative Prediction of Molecular Adsorption: Structure and Binding of Benzene on Coinage Metals, Phys. Rev. Lett. 115 (2015) 036104.

[89] A. Tkatchenko, A. Ambrosetti, R. A. Distasio, Interatomic methods for the dispersion energy derived from the adiabatic connection fluctuation-dissipation theorem, J. Chem. Phys. 138 (2013) 074106.

[90] A. Ambrosetti, A. M. Reilly, R. A. Distasio, A. Tkatchenko, Long-range correlation energy calculated from coupled atomic response functions, J. Chem. Phys. 140 (2014) 18A508.

[91] Y. S. Dedkov, M. Fonin, U. Rüdiger, C. Laubschat, Rashba effect in the graphene/Ni(111) system, Phys. Rev. Lett. 100 (2008) 1.

[92] L. Kong, C. Bjelkevig, S. Gaddam, M. Zhou, Y. H. Lee, G. H. Han, H. K. Jeong, N. Wu, Z. Zhang, J. Xiao, P. a. Dowben, J. a. Kelber, Graphene/substrate charge transfer characterized by inverse photoelectron spectroscopy, J. Phys. Chem. C 114 (2010) 21618. doi:10.1021/jp108616h.

[93] A. Tamtögl, E. Bahn, J. Zhu, P. Fouquet, J. Ellis, W. Allison, Graphene on Ni(111): Electronic Corrugation and Dynamics from Helium Atom Scattering, J. Phys. Chem. C 119 (2015) 25983.